The Radical Cation and Lowest Rydberg States of 1,4-Diaza[2.2.2]bicyclooctane (DABCO)

Gurusamy Balakrishnan,[†,#] Tamás Keszthelyi,[†,‡] Robert Wilbrandt,*[,†,§] Jurriaan M. Zwier,[||] Albert M. Brouwer,[||]* and Wybren Jan Buma[⊥]

Condensed Matter Physics and Chemistry Department, Risø National Laboratory, 4000 Roskilde, Denmark, Institute of Molecular Chemistry, Laboratory of Organic Chemistry, and Laboratory of Physical Chemistry, University of Amsterdam, Nieuwe Achtergracht 129, 1018 WS Amsterdam, The Netherlands

Received: August 26, 1999; In Final Form: November 17, 1999

The radical cation and the two lowest excited singlet Rydberg states of DABCO (1,4-diazabicyclo[2.2.2]-octane) are studied. Experimentally, the radical cation of DABCO is generated by either laser flash photolysis in solution at room temperature or by γ-irradiation in a Freon glass at 77 K, and its electronic absorption and resonance Raman spectra in these two media are reported. The present resonance Raman spectra differ substantially from previous reports given in the literature, and it is concluded that a number of bands attributed previously to the DABCO radical cation are due to other species. Theoretically, the absorption and resonance Raman spectra are interpreted on the basis of density functional theory (DFT; B3LYP/6-31G(d)) calculations and wave packet propagation methods. The same DFT calculations are used to interpret excitation and multiphoton ionization spectra of the two lowest singlet Rydberg states, making use of the close similarity between a Rydberg state and its ionic core. From the combined results it is concluded that DFT calculations with a relatively modest basis set provide a valuable framework to predict potential energy surfaces of radical cations and Rydberg states in terms of minima and Hessians.

I. Introduction

The structural changes that occur upon electronic excitation of a molecule or transfer of an electron in a (weakly coupled) electron donor−acceptor system play an important role in determining the probability or rate of the transfer process. Changes in the normal modes and vibrational frequencies normally contribute less to the overall Franck−Condon factor. For the case of an electron transfer process, $D + A \rightarrow D^{+\cdot} + A^{-\cdot}$, it is important to be able to assess the potential energy surfaces of the electron donor D, its radical cation $D^{+\cdot}$, the electron acceptor A, and its radical anion $A^{-\cdot}$. Current computational techniques, in particular density functional ab initio methods, appear to be quite successful in correctly describing the relevant potential energy surfaces (PES).[1−4] In the present work we compare the results of ab initio calculations of the potential energy surfaces of the electron donor 1,4-diazabicyclo-[2.2.2]octane (DABCO) and its radical cation with several types of spectroscopic data. Obviously, a successful comparison serves not only to validate the computed data but also to allow a detailed interpretation of the experimental data.

In principle, gas phase vibrational data are the most useful to test the quality of theoretical calculations. High-resolution gas phase studies of a radical cation are inherently difficult to perform because it is hard to generate such species in well-defined rovibrational states. Rydberg states may offer a valuable alternative to obtain information on properties of the ground states of radical cations, such as geometry and vibrational force fields, because these properties are not expected to be strongly influenced by the Rydberg electron, which is only weakly bound to the ionic core. Alternatively, vibrational spectra in the condensed phase such as resonance Raman (RR) spectra of the radical cation generated in solution or in a matrix may serve as the experimental basis. On the theoretical side, the study of Rydberg states is difficult, while investigations of the equilibrium structure(s) and vibrations of radical cations are feasible. The difficult part in the analysis of RR spectra is the theoretical assessment of RR intensities which requires knowledge of the potential energy surfaces of higher excited states.

In previous studies, we have investigated the Rydberg states of the rigid cage amines 1-aza[2.2.2]bicyclooctane and 1-azaadamantane,[5,6] and the radical cation of a semiflexible 1,4-diamine, *N*,*N*-dimethylpiperazine.[2,7] Unfortunately, the comparison between Rydberg and radical cation states could not be fully explored on an experimental basis in these cases, because high-resolution spectra were available for only one of the two types of states in each case. For the rigid cage diamine DABCO, which combines the structural features of the above-mentioned molecules, vibrationally resolved spectra have been reported of the lowest Rydberg states and of the radical cation in supersonic expansions.[8] The radical cation ($DABCO^{+\cdot}$) has also been studied in liquid solution using optical absorption and RR spectroscopy,[9,10] but because the spectra reported did not agree with those obtained for the isolated molecule and the results of our calculations, we remeasured them in the present work.

The present paper first describes a combined experimental and theoretical effort to characterize the radical cation $DABCO^{+\cdot}$. While previous RR experiments were carried out by chemical oxidation in a flow experiment, our results are based on a 2-fold approach: (i) direct photooxidation in solution and (ii) oxidation by γ-irradiation in a Freon matrix. It is demonstrated that previously reported RR spectra were due to a mixture of $DABCO^{+\cdot}$ and at least one additional unknown species, while the interpretation was based on the presence of $DABCO^{+\cdot}$ alone. Also, the present theoretical treatment, based on DFT calcula-

* Corresponding author. Fax: +31 20 5255670. E-mail: fred@org.chem.uva.nl

† Risø National Laboratory.

‡ Present address: Department of Chemistry, University of Aarhus, Langelandsgade 140, 8000 Århus C, Denmark.

§ Present address: Bornholms Amtsgymnasium, Søborgstræde 2, 3700 Rønne, Denmark.

|| Institute of Molecular Chemistry, University of Amsterdam.

⊥ Laboratory of Physical Chemistry, University of Amsterdam.

Present address: Department of Chemistry, Princeton University, Princeton, NJ 08544.

10.1021/jp993052n CCC: $19.00
Published on Web 02/10/2000

tions as compared to previous INDO results,[9] provides a much more reliable theoretical basis for assignments of vibrational bands. A substantial revision of the previous interpretation of the RR spectrum is thus necessary. By means of wave packet propagation calculations we interpret the observed RR intensities of $DABCO^{+\cdot}$ which further support the validity of the computed PES.

As an alternative approach, experimental work on Rydberg states offers a means to investigate the ground state of the radical cation. In the present paper this approach is employed to reconsider the results of previous studies on the lowest Rydberg states of DABCO. The vibrational properties of these states were reported previously[8,11−13] in detail using various types of high-resolution excitation spectroscopy, but the present work shows that some revision of the assignments is necessary. Experimental[11,13] and theoretical studies[14,15] have shown that the first excited singlet state (S_1) is the $2\ ^1A_1'$ Rydberg state that arises from the excitation of an electron from the HOMO to the 3s Rydberg orbital. The transition from the ground state to this state is one-photon forbidden but two-photon allowed, whereas the transition to the second excited singlet state (S_2) ($1\ ^1E'$ (HOMO→3p)) is one-photon allowed as well as two-photon allowed under D_{3h} restrictions. From the combination of our experimental results on $DABCO^{+\cdot}$ in different matrices, our DFT calculations, and the previously published gas phase data, a consistent picture emerges of the vibrational properties of the radical cation and the related Rydberg states.

II. Experimental and Computational Methods

A. Materials. 1,4-Diazabicyclo[2.2.2]octane was obtained from Aldrich (no. D2,780−2) and used as received. Water used was of Millipore grade. The solvents $CFCl_3$ (Freon-11, Aldrich) and $BrCF_2CF_2Br$ (Freon-114B2, Fluorochem) were dried on 5 Å molecular sieves. Spectroscopic grade CH_3CN (Merck) was used as received.

B. Experimental Methods. Time-resolved absorption measurements were carried out by laser flash photolysis in solution at room temperature. Aerated CH_3CN solutions of DABCO (4.4×10^{-4} M), contained in a quartz cell of 10×10 mm^2, were photoionized by a laser pulse at 248 nm (80 mJ, 20 ns) from an excimer laser (Lambda Physik LPX 220i). The transient absorption at right angles to the exciting laser beam was monitored by means of a pulsed Xe lamp (Varian VIX150UV), a monochromator (McPherson 2035), and a photomultiplier (1P28). Transient data were stored on a digital oscilloscope (LeCroy 9450) and handled in a PC.

For time-resolved resonance Raman (TRRR) measurements in solution, aerated aqueous or CH_3CN solutions of DABCO (5×10^{-2} M), contained in a rotating cylindrical quartz cell of 3 cm inner diameter, were irradiated by a pulse (248 nm, 10 mJ, 20 ns) from the above-mentioned excimer laser. RR spectra of the short-lived radical cations in the spectral region 200−1800 cm^{-1} were generated 50−100 ns after the photolyzing light pulse at a wavelength of 460 nm (Continuum, Sunlite OPO, 5.0 mJ, 5 ns). The OPO (optical parametric oscillator) was pumped by the third harmonic of a Nd:YAG laser (Continuum, Powerlite − PL9010). The excimer pump and OPO probe lasers were operated at 10 Hz, and the time delay between the pulses was controlled by a digital time delay generator (Stanford DG535). Scattered light was collected at right angles to the exciting probe laser beam, passed through a band-pass filter (Schott WG 360) and a polarization scrambler, and dispersed in a single monochromator (Jobin Yvon − T64000) equipped with a 1200 grooves/mm grating. A back-illuminated liquid N_2 cooled charge coupled device (CCD) with 1100×330 pixels (Princeton Instruments) was used as the multichannel detector. The wavenumber scale was calibrated using Raman bands from cyclohexane as a reference. A sample was exposed to 2000 laser pulses, and spectra from five samples were averaged. The final spectra were obtained after subtraction of both neutral DABCO and solvent bands. The spectra were not corrected for the absorption of the WG-filter, the transient absorption of the sample, and the wavelength dependence of the sensitivity of the detection system. Optical absorption spectra of the solutions before and after each TRRR measurement were compared, and no detectable photoproducts were observed. Neither were any new Raman bands from photoproducts observed after the transient experiments.

Alternatively, radical cations were produced by γ-irradiation in Freon glasses at 77 K. For these measurements, 2×10^{-2} M solutions of DABCO in an air saturated 1:1 (v/v) mixture of $CFCl_3$ and $BrCF_2CF_2Br$ were prepared. Upon cooling to 77 K the samples formed transparent glasses. For measuring electronic absorption spectra, the glasses were irradiated with a dose of 0.05 Mrad by ^{60}Co γ-rays, while doses of 0.4 Mrad were used for the resonance Raman. The samples were then transferred to an Oxford Instruments DN1704 liquid nitrogen cryostat to perform the optical measurements. The samples were prepared in 10 mm inner diameter cylindrical and 10×10 mm^2 rectangular quartz cells to record RR and electronic absorption spectra, respectively. During the RR measurements, the cells were rotated at 8 rpm in the cryostat. Raman spectra were recorded in backscattering geometry, using a triple (consisting of a subtractive double and a single) monochromator (Jobin-Yvon T64000) and an intensified diode array (Spectroscopy Instruments).

C. Theoretical Methods. Ab initio calculations were carried out using the *Gaussian* suite of programs.[16] Hartree−Fock (HF) calculations and DFT calculations using the BLYP and B3LYP density functionals[17−19] were carried out. The standard 6-31G(d) or 6-311G(d) basis sets were used. Because the excited state of the radical cation is the lowest state of A_2'' symmetry, single-determinantal methods could be used to obtain its energy, the gradient components, and the force constants, at least for the totally symmetric coordinates.

The procedures for calculating optical absorption and RR spectra have been described in detail in two recent papers.[2,7] Here we adopt the *vertical Hessian approximation*, based on the wave packet formalism developed by Tannor and Heller.[20] In their formulation the vibrational Hamiltonians are written in terms of dimensionless normal coordinates. Each of the potential surfaces of the vibrational Hamiltonians is characterized by a set of normal coordinates and harmonic vibrational frequencies. The relative position of the potential surfaces involved in the optical processes is characterized by the Duschinsky rotation matrix and a set of dimensionless displacements. In the following, the parameters, which characterize the potential surfaces and their relative positions, are referred to as the *vibrational parameters*.

In the present work, the vibrational parameters of the radical cation of DABCO have been obtained by use of quantum chemical DFT calculations. Assuming harmonic potentials for the two electronic states involved in the resonance transition, the vertical Hessian approximation uses the molecular gradient and Hessian of the excited electronic state, evaluated at the optimized geometry of the ground electronic state, together with the Hessian of the ground electronic state, evaluated at the same geometry. In this approach both the ground and excited state

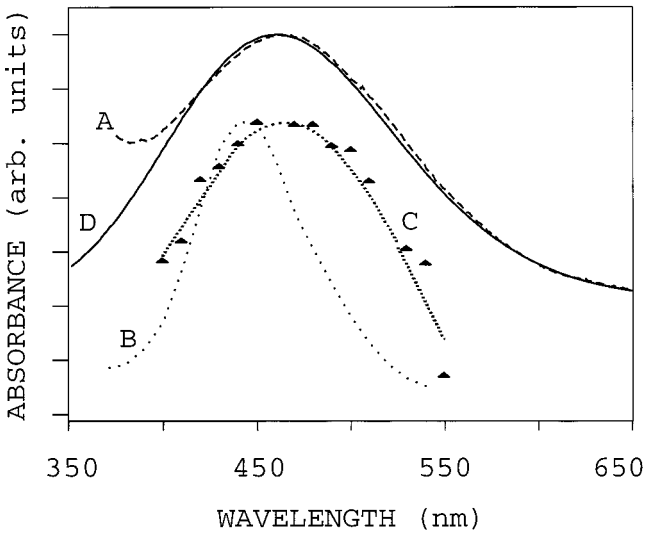

Figure 1. Experimental and calculated electronic absorption spectra of $DABCO^{+\cdot}$. (A) Observed spectrum in a Freon matrix at 77 K, after γ-irradiation of a 2×10^{-2} M solution of DABCO. (B) Spectrum in acetonitrile at room temperature (from ref 21). (C) Spectrum in acetonitrile at room temperature, obtained 30 ns after irradiation by a laser pulse (248 nm) from an excimer laser (this work). (D) Calculated spectrum (see text for details) modeling spectrum A. Spectra A and D are vertically offset with respect to B and C.

potential surfaces are expanded to second order in the nuclear coordinates around the same point, i.e., the optimized geometry of the ground electronic state. The vibrational parameters obtained in this way are then used as input parameters for the evaluation of optical absorption spectra and resonance Raman intensities by means of wave packet propagation techniques.

III. Experimental Absorption and Resonance Raman Spectra of $DABCO^{+\cdot}$

Observed electronic absorption spectra of the radical cation of DABCO are shown in Figure 1.

Spectrum A was recorded in a Freon glass at 77 K after γ-irradiation, spectrum B is the time-resolved spectrum in solution at room temperature, as reported by Halpern et al.,[21] spectrum C was constructed from our transient absorption data 30 ns after photoionization of a CH_3CN solution of DABCO at room temperature. Spectrum D is the calculated spectrum (see below), simulating the observed spectrum A.

The experimentally observed spectrum in the Freon glass (A) is very similar to the one reported by Shida et al.,[22] thus confirming that under our experimental conditions the DABCO radical cation is produced. The experimentally observed spectrum in solution (C) is in qualitative agreement with that reported previously (B),[21] but it is slightly red shifted and broader.

The resonance Raman spectrum of $DABCO^{+\cdot}$ has been reported previously by Hester and co-workers.[9] In that work, DABCO was mixed with NaOCl (hypochlorite) in a stopped or continuous flow experiment. RR spectra were recorded from the reaction mixture, and bands assigned to $DABCO^{+\cdot}$ were reported at 1563, 1358, 1279, 999, 983, 884, 809, 792, 679, 643, and 140 cm^{-1}. Two additional modes with frequencies of 435 and 330 cm^{-1} were not observed directly, but inferred from putative overtones.

The molecule having D_{3h} symmetry, of the 36 normal modes ($6a_1' + 3a_2' + 4\,a_1'' + 5a_2'' + 9e' + 9e''$) of $DABCO^{+\cdot}$, 29 are IR and/or Raman active ($6a_1' + 5a_2'' + 9e' + 9e''$). In the absence of vibronic coupling or changes of point group upon excitation, only the six totally symmetric modes are expected to be active

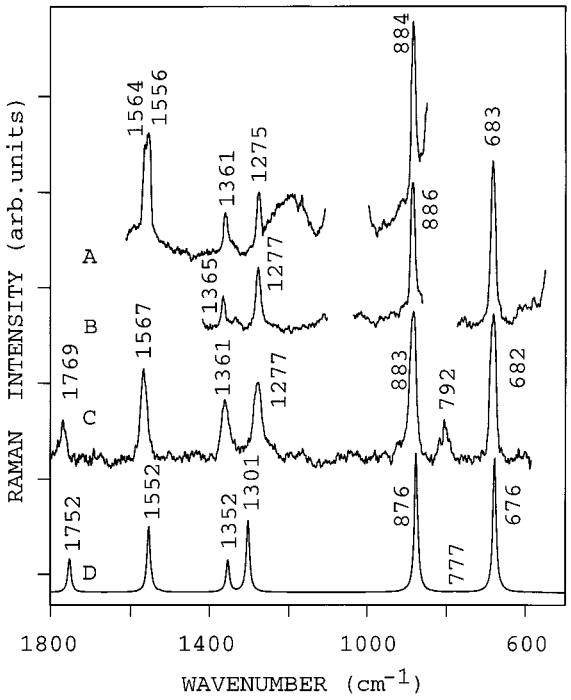

Figure 2. Observed and calculated resonance Raman spectra of $DABCO^{+\cdot}$. (A) Observed spectrum at 77 K after γ-irradiation of a 2×10^{-2} M solution of DABCO in an air saturated 1:1 (v/v) mixture of $CFCl_3$ and $BrCF_2CF_2Br$. (B) As spectrum A, however in pure $CFCl_3$. (C) TRRR spectrum of $DABCO^{+\cdot}$ in acetonitrile at room temperature, obtained 100 ns after irradiation of a 5×10^{-2} M solution with a laser pulse at 248 nm. Excitation wavelength for all spectra 460 nm. (D) Calculated resonance Raman spectrum of $DABCO^{+\cdot}$ based on DFT and wave packet propagation methods using the vertical Hessian approach (see text for details).

in the resonance Raman spectrum. The large number of bands observed and assigned to $DABCO^{+\cdot}$ by Ernstbrunner et al.[9] was thus remarkable and called for further attention. Some bands were attributed to Fermi resonances and some remained unexplained. In light of that work we decided to remeasure the RR spectrum of $DABCO^{+\cdot}$.

The resonance Raman spectra of $DABCO^{+\cdot}$ measured in the present study are shown in Figure 2. Figure 2A shows the spectrum excited in the glass formed by the Freon mixture, Figure 2B is obtained from a glass using one Freon component only ($CFCl_3$), Figure 2C is recorded in aqueous solution at room temperature, and finally, Figure 2D shows the calculated spectrum (see below). Observed and calculated vibrational wavenumbers are listed in Table 1. The experimental spectra are in good agreement with each other. Blank domains in spectra 2A and 2B correspond to spectral regions masked by strong vibrational bands of the Freon matrix.

It can be noted that the observed RR spectra of the present work show considerably fewer bands than those previously reported,[9] but that the band positions of the observed bands are in good agreement with previously reported data. Such a situation could in principle be explained by the different excitation wavelengths used. Previous experiments used 476.2 and 488 nm excitation, respectively,[9,10] while our excitation wavelength was 460 nm. While changes in relative intensities usually do occur with varying excitation wavelength, the reported differences for 476.2 and 488 nm excitation were small. Taking further into account that the $DABCO^{+\cdot}$ absorption spectrum is broad and structureless, it seems highly unlikely that the substantial differences between our work and previous RR spectra can be ascribed to the different excitation wave-

TABLE 1: Observed and Calculated (a_1' modes only) Vibrational Frequencies (cm^{-1}) of the Radical Cation $DABCO^{+\cdot}$ Obtained from Resonance Raman Spectra and B3LYP/6-31G(d) Calculations

experiment			calculations		
in H_2O (this work)	Freon glass[a]	in H_2O (ref 9)	wavenumber (cm^{-1})[c]	mode number	mode description
			3041	ν_1	νC−H
1769			1752	2 ν_4	
1567	1564	1563	1552	$\nu_4+\nu_6$	
	1556		1523	ν_2	δCH_2
1361	(1365) 1361	1358	1352	2 ν_6	
1277	(1277) 1275	1279	1301	ν_3	wCH_2/ν_{CC}
		999			
			983		
883	(886) 884	884	876	ν_4	νCC/ wCH_2
		809			
[792][b]		792	777	ν_5	ν_sNC3
682	(683)	679	676	ν_6	δCCC
		643			
		[435][b]			
		[330][b]			
		140			

[a] Data from two different matrices: matrix A, consisting of a 1:1 (v/v) mixture of $CFCl_3$ and $BrCF_2CF_2Br$ and matrix B (in parentheses) consisting of $CFCl_3$ only. [b] Doubtful. [c] Scaled by factor 0.974.

TABLE 2: Experimental and Calculated ((U)B3LYP/6-311G(d)) Structural Data of DABCO and Its Radical Cation $DABCO^{+\cdot}$

	neutral ground state S_0 (exptl)[b]	neutral ground state S_0 calcd[a]	S_1 state calcd	radical cation calcd
CC bond (Å)	1.562 ± 0.009	1.565 (1.556)	1.648	1.639
CN bond (Å)	1.472 ± 0.007	1.473 (1.459)	1.438	1.438
CH bond (Å)	1.110 ± 0.01	1.094 (1.085)	1.093	1.089
CNC angle (°)	108.7 ± 0.4	108.9 (109.1)	112.6	112.1
CCN angle (°)	110.2 ± 0.4	110.1 (109.8)	106.0	106.7

[a] Values in parentheses from HF/6-31G(d). [b] Reference 23. [c] The structure of the molecule in the S_1 state was derived using the D_0 force field and the experimentally observed intensities for the transitions in the two-photon $S_0 \rightarrow S_1$ excitation spectrum.[11]

lengths. We thus conclude that previous spectra, obtained from a reacting mixture, were due to the presence of $DABCO^{+\cdot}$ together with at least one unknown additional species apparently having an optical transition in the blue spectral region and therefore being in resonance with the exciting laser light. Hence, the previous assignments and interpretation in terms of calculated normal modes of vibration are revised in the present work.

IV. Computational Results and Discussion

A. Geometric and Electronic Structure of DABCO and $DABCO^{+\cdot}$. Molecular structure parameters calculated using D_{3h} symmetry for the neutral ground state of DABCO, and its radical cation ($DABCO^{+\cdot}$), are listed in Table 2. The agreement of the computed structure of the neutral molecule with the gas phase electron diffraction results[23] is remarkably good. For the radical cation experimental structure data are not available.

DABCO is a classical example of a molecule in which orbital interactions occur between the amino groups predominantly through the intervening σ-bonds.[24] Its photoelectron spectrum has been interpreted[25] to show that the highest occupied molecular orbital (Figure 3) is the symmetric combination of the nitrogen lone pair orbitals, mixed with the C−C σ-bonding orbitals. The large splitting of the two lone pair orbitals, which raises the HOMO energy, is the reason for the relatively low ionization potential[26] of DABCO. In the neutral molecule this interaction is in fact energetically slightly unfavorable, but it is enforced by the molecular framework. When an electron is removed from the HOMO, the net effect of the interaction between the amino lone pairs is highly favorable, which explains the low oxidation potential of DABCO.[27]

Removal of an electron from an orbital which has σ-bonding character obviously weakens the C−C bonds. According to our calculation, they lengthen from 1.57 Å to as much as 1.64 Å, whereas the C−N bonds are shortened from 1.47 to 1.44 Å. Removal of an electron from an amine lone pair orbital leads to a flattening of the amino group. This can be characterized by the increase of the C−N−C bond angles, in this case from a nearly tetrahedral value of 109° to 112°. Interestingly, this increase is about half of the increase in the monoamine ABCO (1-azabicyclo[2.2.2]octane),[6] where one electron is removed from a single lone pair, while in DABCO one electron is removed from a set of four lone pair electrons, and the unpaired electron density is shared by the two equivalent amino centers.

B. Optical Absorption Spectrum of $DABCO^{+\cdot}$. While neutral DABCO does not show any visible electronic absorption bands, the radical cation $DABCO^{+\cdot}$ shows an absorption band (see Figure 1) with a maximum around 465 nm. The removal of an electron from the HOMO does not change the spatial symmetry of the molecular electronic wave function, thus the ground state of the radical cation has A_1' symmetry. The lowest energy $A_1' \rightarrow A_2''$ transition involves a simple one-electron excitation from the antisymmetrical a_2'' HOMO-1 to the symmetrical a_1' HOMO (Figure 3). The vertical transition energy calculated at the B3LYP/6-31G(d) level is 2.64 eV (469.7 nm), in excellent agreement with the observed value.

To simulate the electronic absorption spectrum, the ground and excited electronic potential surfaces have to be calculated. As described above, for the case of $DABCO^{+\cdot}$ the simulations have been performed within the vertical Hessian approximation. This involves the determination of the vibrational parameters, i.e., gradient and Hessian of both states at the equilibrium geometry of the ground state and then the evaluation of dimensionless displacements and the Duschinsky rotation matrix between the two states. The calculated harmonic frequencies

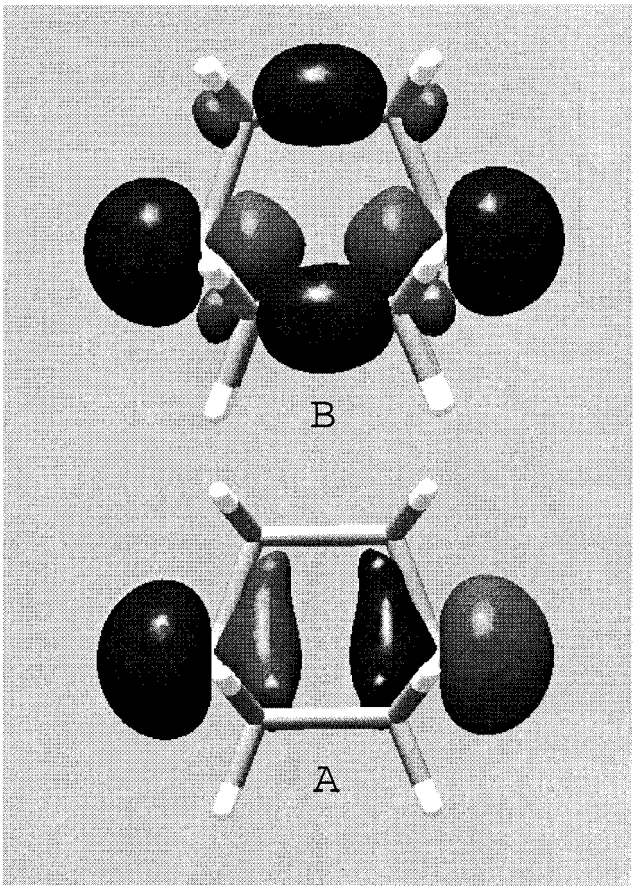

Figure 3. Calculated (B3LYP/6-31G(d)) HOMO-1 (A) and HOMO (B) orbitals of neutral DABCO.

TABLE 3: Calculated Vibrational Frequencies (cm^{-1}) (UB3LYP/6-31G(d), scaled × 0.974) of $DABCO^{+\cdot}$ in the Ground State $A_1'(\nu_g)$ and the Lowest Excited State A_2'' (ν_e) with Calculated Dimensionless Displacements (vertical Hessian approach)

mode	ν_g	ν_e	displacement
ν_1	3041	3034	−0.026
ν_2	1523	1504	0.050
ν_3	1301	1347	−0.911
ν_4	876	927	1.527
ν_5	777	754	0.759
ν_6	676	440	−6.220

and displacements are listed in Table 3. All frequencies were scaled by a factor of 0.974.[2] As discussed previously,[7] it should be noted that the listed displacements do not necessarily represent the true displacements of the minima of the two potential energy surfaces. Only in the case of a strictly harmonic excited state potential energy surface the true minimum and the one corresponding to the vertically calculated displacements are identical.

When simulating the observed electronic absorption spectrum, two parameters, namely the transition energy E_0 and the homogeneous bandwidth Γ of the excited electronic state, are fitted to produce the best possible agreement with experiment. For the calculated spectrum of Figure 1D (simulating the absorption spectrum observed in the Freon matrix, Figure 1A), values of 11900 and 500 cm^{-1} were used for E_0 and Γ, respectively. From a comparison of calculated and observed spectra, it is seen that excellent agreement is obtained. For the solution spectra, the narrower width of the absorption band observed by Halpern et al. (Figure 1B) could not be reproduced by simulations, even using smaller values of Γ. Moreover, smaller Γ's introduced substantial vibronic structure in the absorption spectrum. The value of $\Gamma = 500$ cm^{-1} is rather large and corresponds to an excited state lifetime of only 67 fs. The experimental spectra were, however, measured in condensed phases, so the associated inhomogeneous broadening is effectively taken into account by the Γ parameter as well.

C. Vibrational Spectra of Neutral DABCO. The ground state vibrational frequencies of DABCO have been reported by different groups. In Table 4 we compile the values from the most recent source, i.e., the fluorescence study of Consalvo et al.,[12] supplemented with data from the literature cited by the same authors, and the Raman and infrared study of Ernstbrunner et al.[9] The vibrational frequencies calculated at the B3LYP/6-31G(d) and HF/6-31G(d) levels, with frequencies scaled by a standard factor of 0.974 (B3LYP) and 0.9 (HF), are in good agreement with the experimental ones. Compared to earlier assignments,[9] a few changes should be noted: the observed Raman band at 1458 cm^{-1} was previously assigned to the totally symmetric ν_2 mode. However, in the light of the calculated Raman intensities, together with the observed depolarization ratio, an assignment to ν_{21} and/or ν_{30} (both CH_2 wag modes) seems much more likely. Also the previous assignments of the observed Raman bands at 1328, 1301, and 913 cm^{-1} are modified in the light of the present, more accurate, calculations. Previous infrared assignments are in agreement with ours.

D. Resonance Raman Spectrum of $DABCO^{+\cdot}$. As seen in Figure 2, RR spectra of $DABCO^{+\cdot}$ in the Freon matrix and in solution are very similar. The only notable difference is the observation of two vibrational bands in the region 1556−1564 cm^{-1} in the matrix, while only one (at 1567 cm^{-1}) is found in solution. We attribute this to Fermi resonance between the fundamental ν_2 and the combination $\nu_4 + \nu_6$. As shall be seen below, the calculated intensity of ν_2 is very low and the band observed in solution is therefore most likely assigned to $\nu_4 + \nu_6$. The fact that Fermi resonance is observed in the matrix only is not surprising, as media effects are known to have a strong influence on coupling elements which are operative in Fermi resonance. We hence assign the bands at 1564 (matrix) and 1567 cm^{-1} (solution) to the combination $\nu_4 + \nu_6$ (calculated at 1552 cm^{-1}) and the band at 1556 cm^{-1} (matrix) to the fundamental ν_2 (calculated at 1523 cm^{-1}). The remaining bands are straightforward to assign. Three fundamentals, observed at 1277, 883, and 682 cm^{-1} (solution), are assigned to ν_3, ν_4, and ν_6 (calculated at 1301, 876, and 676 cm^{-1}). The ν_5 mode is not observed in the resonance Raman spectra, but its frequency (788 cm^{-1}) is known from the MPI spectrum (see below). Visual inspection of the normal modes shows that ν_5 in the ground state of the neutral (805 cm^{-1}) can be characterized as a C−N stretching vibration, and that ν_4 (985 cm^{-1}) involves predominantly C−C stretching character. On account of the stiffening of the C−N bonds and the weakening of the C−C bonds we thus would expect that upon ionization ν_5 and ν_4 would increase and decrease in frequency, respectively. The bands observed at 788 and 883 cm^{-1} for the radical cation would accordingly be assigned as ν_5 and ν_4. The Duschinsky matrix for the a_1' modes of S_0 and D_0 (not shown) demonstrates, however, that the situation is somewhat more complicated since a complete mixing of the two modes occurs upon ionization.

As a result of the rehybridization of the nitrogen atoms, the frequency of the ν_6 mode increases upon ionization − in the ground state of the neutral its frequency is 596 cm^{-1} − similar to what has been observed for the monoamines ABCO and 1-aza-adamantane,[6] although the frequency shift is considerably smaller in the latter two molecules.

TABLE 4: Observed and Calculated (B3LYP/6-31G(d) and HF/6-31G(d)) Vibrational Frequencies (cm^{-1}) of Neutral DABCO

						HF/6-31G(d)[d]			
no.	symmetry	LIF[a]	Raman[b]	IR[b]	B3LYP[c]	freq	IR intensity	Raman intensity	assignment
ν_1	a_1'	2873			2975	2914		462.0	νCH_2
ν_2	a_1'	1462			1485	1505		2.6	δCH_2
ν_3	a_1'	1327	1352		1343	1368		4.5	ρCH_2
ν_4	a_1'	958	983		942	955		24.4	νCC
ν_5	a_1'	805[e]	806		792	790		29.7	νNC_3
ν_6	a_1'	596	630		592	589		0.2	νNC_3
ν_7	a_2'				3014	2938			νCH_2
ν_8	a_2'				1177	1171			ρCH_2
ν_9	a_2'				796	789			ρCH_2
ν_{10}	a_1''				2993	2916			νCH_2
ν_{11}	a_1''				1246	1248			ρCH_2
ν_{12}	a_1''				1011	1018			ρCH_2
ν_{13}	a_1''	58[f]			100	74			ρNC_3
ν_{14}	a_2''	2866		2883	2962	2896	142.9		νCH_2
ν_{15}	a_2''	1458[g]		1464	1479	1491	2.7		ρCH_2
ν_{16}	a_2''	1350[g]		1360	1368	1383	10.5		ρCH_2
ν_{17}	a_2''	987[g]		1000	972	970	34.0		δNC_3
ν_{18}	a_2''	749[g]		781	751	765	78.5		νNC_3
ν_{19}	e'	2945		2970	3021	2949	131.6	127.8	νCH_2
ν_{20}	e'	2960[g]		2952	2966	2902	119.4	0.1	νCH_2
ν_{21}	e'	1458	1458	1457	1478	1488	3.8	13.6	ρCH_2
ν_{22}	e'	1320	1320	1322	1330	1343	14.7	4.0	$\nu NC_3/\rho CH_2$
ν_{23}	e'	1292			1313	1320	2.5	0.2	ρCH_2
ν_{24}	e'	1065	1062	1061	1055	1080	52.6	14.7	νNC_3
ν_{25}	e'	892[g]	913	891	876	876	6.9	0.8	νCC
ν_{26}	e'	824	825		812	814	4.8	1.0	ρCH_2
ν_{27}	e'	423	424		417	417	0.0	0.1	δNC_3
ν_{28}	e''				2997	2923		88.1	νCH_2
ν_{29}	e''				2959	2890		44.9	νCH_2
ν_{30}	e''	1448[e]	1458		1469	1475		21.3	ρCH_2
ν_{31}	e''		1328		1326	1344		0.3	ρCH_2
ν_{32}	e''		1301		1308	1308		13.9	ρCH_2
ν_{33}	e''				1185	1204		1.1	ρCH_2
ν_{34}	e''				1017	1030		0.2	νNC_3
ν_{35}	e''	580[g]	577		575	579		4.3	$\delta NCCN$
ν_{36}	e''	335[g]	332		331	326		0.5	δNC_3

[a] Laser induced fluorescence, ref 28. [b] Reference 9. [c] This work, calculation, UB3LYP/6-31G(d), frequencies scaled by 0.974. [d] This work, calculation, HF/6-31G(d), frequencies scaled by 0.90. [e] Values obtained from ref 33. [f] Value obtained from ref 34 [g] Value obtained from ref 35; a_2'' modes from gas-phase IR data.

The two bands at 1769 and 1361 cm^{-1} (solution) are assigned to the overtones 2 ν_4 (1752 cm^{-1}) and 2 ν_6 (1352 cm^{-1}). The calculated spectrum is shown in Figure 2D. It can be concluded that calculated band positions in terms of harmonic frequencies are in good agreement with experimental data. The totally symmetric normal modes of vibration are shown in Figure 4.

E. Resonance Raman Intensities of $DABCO^{+\cdot}$. In the case when the Raman excitation wavelength is in resonance with an electronic dipole allowed transition, Franck−Condon scattering, providing enhancement of totally symmetric modes only, usually represents the dominant scattering mechanism. Either changes in equilibrium geometry between the two resonant electronic states along totally symmetric modes or changes in vibrational frequency upon excitation provide resonance enhancement to these modes and also to their combinations or overtones. Geometry changes are normally by far the dominant mechanism. Since we excite the Raman spectrum of $DABCO^{+\cdot}$ in resonance with the allowed $A_1' \rightarrow A_2''$ electronic transition, RR intensities are expected to mainly reflect the geometrical changes between the ground and excited states. From qualitative considerations, one would thus expect the normal modes having the largest displacements on going from the lower to the upper resonant electronic state to show the greatest resonance enhancement. In reality, however, this qualitative picture must be revised considerably according to our more detailed calculations of resonance Raman spectra. The calculation based on the vertical Hessian approximation reproduces the observed intensity pattern

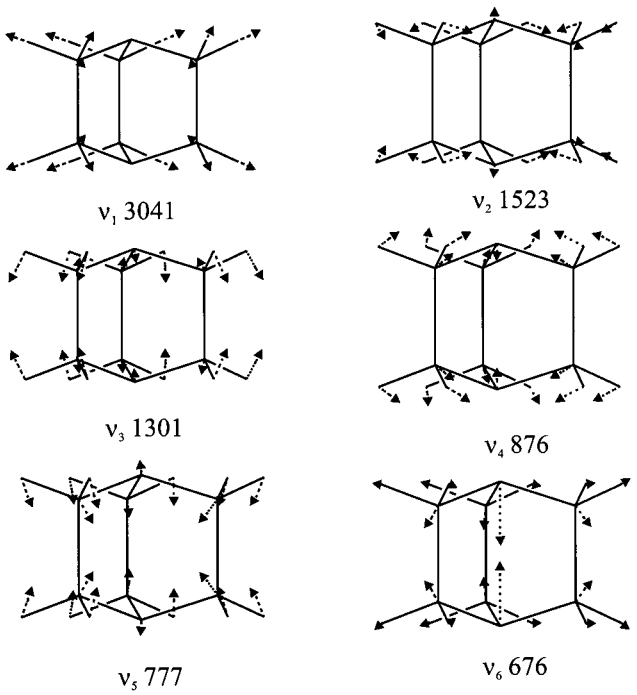

Figure 4. Calculated normal modes of vibrations for the six totally symmetric a_1' modes of $DABCO^{+\cdot}$. Indicated wavenumbers from UB3LYP/6-31G(d) calculations, scaled by a factor of 0.974.

TABLE 5: Observed Vibrational Frequencies (cm^{-1}) of the Radical Cation $DABCO^{+\cdot}$ and the Two Lowest Excited Rydberg States (S_1 and S_2) of DABCO together with Calculated (B3LYP/6-31G(d)) Vibrational Frequencies of $DABCO^{+\cdot}$

mode	symmetry	S_1 (expt)	S_2 (expt)[e]	$DABCO^{+\cdot}$ (gas phase)[f]	$DABCO^{+\cdot}$ (aqueous solution, RR)[g]	$DABCO^{+\cdot}$ (calc)[i]
ν_1	a_1'					3041
ν_2	a_1'				1556[h]	1523
ν_3	a_1'	1258[b]	1293	1277	1277	1301
ν_4	a_1'	883[a]	875	879	883	876
ν_5	a_1'	778[a]	788	788		777
ν_6	a_1'	671[c]	685	680	682	676
ν_7	a_2'					3102
ν_8	a_2'					1162
ν_9	a_2'					816
ν_{10}	a_1''					3086
ν_{11}	a_1''					1171
ν_{12}	a1″					1010
ν_{13}	a1″	99[b]				111
ν_{14}	a2″					3035
ν_{15}	a2″					1501
ν_{16}	a_2''					1328
ν_{17}	a_2''	919[c]		929		914
ν_{18}	a_2''	704[f]		726		731
ν_{19}	e′					3109
ν_{20}	e′					3036
ν_{21}	e′					1484
ν_{22}	e′					1349
ν_{23}	e′			1245		1235
ν_{24}	e′	1011[c]		1014		1012
ν_{25}	e′	825[c,d]		854		852
ν_{26}	e′	684[f]		681		688
ν_{27}	e′	449[a]		453		445
ν_{28}	e″					3091
ν_{29}	e″					3031
ν_{30}	e″					1472
ν_{31}	e″					1339
ν_{32}	e″					1287
ν_{33}	e″					1141
ν_{34}	e″					1055
ν_{35}	e″					544
ν_{36}	e″	352[a]				357

[a] Values obtained from ref 28 with exceptions as noted. [b] Values obtained from ref 11. [c] Values obtained from ref 12. [d] This vibration was assigned as ν_{26} by Consalvo et al.[12] [e] These values were obtained from ref 36. [f] Values obtained from ref 8. [g] This work, aqueous solution, room temperature. [h] In Freon matrix, 77 K. [i] Calculated (B3LYP/6-31G(d)) frequencies scaled × 0.974.

remarkably well, including the intensity of overtones and combinations. The displacements listed in Table 3 would lead one to expect that the strongest Raman band would be ν_6. Experimentally, three strong fundamentals and a number of overtones are observed. Normal mode rotation, in particular involving ν_6, is the main reason for the redistribution of intensity from ν_6 to other modes. Given the good agreement between experiment and theory, and considering the low calculated intensity of ν_2, the above-mentioned assignment of the strong observed bands at 1564 (matrix) and 1567 cm^{-1} (solution) to the combination $\nu_4 + \nu_6$ (calculated at 1552 cm^{-1}) seems by far more likely than an assignment to ν_2, which, based on wavenumbers only, would be another possibility.

F. Rydberg States and MPI Spectrum. Vibrational frequencies have been reported[8] for the S_1 state, the S_2 state, and the ground state of the radical cation of isolated DABCO molecules, which were obtained from two-photon excitation, one-photon excitation, and MPI photoionization spectra, respectively. These data are listed in Table 5.

Having validated the calculated vibrational spectrum of $DABCO^{+\cdot}$ by comparison with the resonance Raman spectra obtained under different experimental conditions, the assignment of four a_1' modes in the MPI spectrum is straightforward, even though the original assignments of Fujii et al.[8] were quite different. All four modes have a counterpart with very similar frequency in the spectra of the S_1 and S_2 states of DABCO.[13,28]

The modes at 726 and 929 cm^{-1} in the MPI spectra agree well with frequencies calculated at 731 and 914 cm^{-1} for a_2'' modes. Also, the bands observed in the MPI spectrum at 1245, 1014, 854, 681, and 453 cm^{-1} are all well described by theoretically calculated e′ modes at 1235, 1012, 852, 688, and 445 cm^{-1}. The lowest excited singlet state is of A_1' symmetry. The one-photon transition to this state is therefore symmetry forbidden and can only occur by vibronic coupling with dipole-allowed states. As yet, the presence of false origins built upon vibrations of e′ symmetry in the one-photon excitation spectrum of S_1 [11] has been taken as evidence that vibronic coupling mainly occurs with states of E′ symmetry, most probably S_2.[13] Our assignment of the two a_2'' modes implies that S_1 is also subject to vibronic coupling with states of A_2'' symmetry. Based upon energy arguments, the dominant coupling is expected to be with S_3, associated with excitation to a $3p_z$ Rydberg orbital.[14,15]

On the basis of the assumption that S_1 has the same equilibrium geometry and force field as D_0, predictions have been made of the transition intensities to vibrational levels of a_1' symmetry in the excited state for the two-photon allowed excitation spectrum of the $S_1 \leftarrow S_0$ transition. To this purpose vibrational overlap integrals have been calculated employing the theory as developed in ref 29. In Table 6 the results of these predictions are given and compared with experimentally obtained intensities. It is clear that the computed intensities are in good agreement with the experimental results, although some minor differences remain. Part of these differences might be attributed to an inaccurate Duschinsky matrix, but of much more

TABLE 6: Assignments and Intensities for the Major Bands in the DABCO $S_1 \leftarrow S_0$ Two-Photon Excitation Spectrum[a]

relative energy (exp)[b]	relative ntensity (exp)[c]	relative energy (calc)[g]	relative intensity (calc)[g]	assignment
0	100	0	100.0	0_0^0
204	*d*	215	1.5	13_0^2
671[f]	*d*	679	4.5	6_0^1
778	125	776	83.1	5_0^1
883	116	876	123.0	4_0^1
1258	115	1302	61.4	3_0^1
1449[e]	*d*	1454	6.4	$6_0^1 5_0^1$
1552	85	1551	31.8	5_0^2
1554[e]	*d*	1555	6.6	$6_0^1 4_0^1$
1656	72	1652	94.6	$5_0^1 4_0^1$
1766	37	1753	76.5	4_0^2
1929[e]	*d*	1981	3.3	$6_0^1 3_0^1$
2039	26	2078	48.6	$5_0^1 3_0^1$
2138	91	2179	74.4	$4_0^1 3_0^1$
2227[e]	*d*	2230	3.8	$5_0^2 6_0^1$
2329	27	2328	7.4	5_0^3
2432	49	2427	33.2	$5_0^2 4_0^1$
2437[e]	*d*	2432	4.8	$4_0^2 6_0^1$
2513	18	2604	18.0	3_0^2
2544[e]	30	2529	54.3	$4_0^2 5_0^1$
2642	9	2630	32.0	4_0^3

[a] All energies are given in cm^{-1} with respect to the transition energy of the 0−0 transition, whose intensity has been taken as 100. [b] Data from ref 11. [c] Estimated intensities (±5%) from Figure 2a of ref 11. [d] Low intensity bands. Relative intensities between 0 and 10%. [e] Exact energy not given by Gonohe et al.[11] These values are estimates based on the vibrational frequencies. [f] From Consalvo et al.[12] [g] B3LYP/6-311G(d).

influence are differences in the geometries of S_1 and D_0, which, even for small changes, lead to substantial variations in the intensities. If indeed these geometrical factors are the dominant cause for the differences between calculated and observed intensities, it is possible to reconstruct the equilibrium geometry of the lowest excited singlet state from the experimentally observed transition intensities.[29] Implicit in such a treatment is the assumption that the force fields and geometries of S_0 and D_0 have been calculated "exactly". The results of such a reconstruction have been given in Table 2, from which it can be concluded that the equilibrium geometries of S_1 and D_0 differ only slightly.

G. Reorganization Energies. The rate of an electron transfer process is determined by several important factors, such as electronic coupling, driving force, solvent reorganization energy, and internal reorganization energy. Changes in the experimental variables of a system under study often affect more than one of these theoretical parameters at the same time. The internal reorganization energy is probably relatively insensitive to external perturbations, so it should be relatively easy to deal with. Unfortunately, direct experimental determination is rarely possible. The difference between vertical and adiabatic ionization potentials, for example, can only be determined in a reliable way for a well-resolved photoelectron spectrum, while many interesting electron donors have broad unresolved spectra with overlapping bands. Therefore, for many electron donors considerable uncertainty exists,[30,31] and accurate theoretical calculations may be helpful here.[1,2] In the present case of DABCO, a reasonably accurate experimental estimate of $\lambda_i = 0.32$ eV can be based on the difference in the vertical and adiabatic ionization energies ($IP_v = 7.52$ eV,[26] $IP_a = 7.20$ eV[8]). The computed value is 0.33 eV, in excellent agreement. This supports the idea that the B3LYP density functional method with a modest basis set such as 6-31G(d) may be a generally adequate level for the calculation of reorganization energies.[32]

V. Conclusions

On the basis of remeasured resonance Raman spectra of the radical cation of DABCO, together with spectroscopic data reported previously in the literature on DABCO and $DABCO^{+\cdot}$, we have shown that DFT calculations on neutral DABCO and its radical cation allow the elucidation of the geometric and vibrational properties of the molecule in these two oxidation states. It is concluded that previously reported resonance Raman spectra of $DABCO^{+\cdot}$ were contaminated with vibrational bands from other unknown species. New assignments have been offered for a number of vibrational bands. It has been demonstrated that the present calculations are able to model impressively the vibrational frequencies and transition intensities in the resonance Raman spectrum (including overtones and combinations) of $DABCO^{+\cdot}$ as well as in the excitation spectra of the lower excited Rydberg states. Comparison between experimentally observed and theoretically calculated intensities has allowed the determination of the geometry differences between the ground state of the radical cation and the lowest excited Rydberg state. These results suggest that vibronic spectra of Rydberg states, which form a considerable challenge from a computational point of view, can be well studied employing relatively inexpensive calculations on the ionic manifold. On the other hand, for molecules where high-resolution spectroscopic data on the ionic manifold are difficult to obtain, spectroscopy on Rydberg states can be used to advantage to unravel the properties of the ionic core upon which these Rydberg states are built.

Acknowledgment. This research was sponsored by the "Stichting Nationale Computer Faciliteiten" (National Computing Facilities Foundation, NCF), and by The Netherlands Foundation for Chemical Research (SON), with financial support from the "Nederlandse Organisatie voor Wetenschappelijk Onderzoek" (Netherlands Organization for Scientific Research, NWO). Furthermore, this work was supported by a grant from the Danish Natural Science Research Council to the Center for Molecular Dynamics and Laser Chemistry.

References and Notes

(1) Nelsen, S. F.; Blackstock, S. C.; Kim, Y. *J. Am. Chem. Soc.* **1987**, *109*, 677.

(2) Brouwer, A. M.; Zwier, J. M.; Svendsen, C.; Mortensen, O. S.; Langkilde, F. W.; Wilbrandt, R. *J. Am. Chem. Soc.* **1998**, *120*, 3748.

(3) Brown, S. T.; Rienstra-Kiracofe, J. C.; Schaefer, H. F. *J. Phys. Chem. A* **1999**, *103*, 4065.

(4) Grafton, A. K.; Wheeler, R. A. *J. Phys. Chem. A* **1997**, *101*, 7154.

(5) Zwier, J. M.; Brouwer, A. M.; Rijkenberg, A.; Buma, W. J. *J. Phys. Chem. A* **2000**, *104*, 729.

(6) Zwier, J. M.; Wiering, P. G.; Brouwer, A. M.; Bebelaar, D.; Buma, W. J. *J. Am. Chem. Soc.* **1997**, *119*, 11523.

(7) Brouwer, A. M.; Svendsen, C.; Mortensen, O. S.; Wilbrandt, R. *J. Raman Spectrosc.* **1998**, *29*, 439.

(8) Fujii, M.; Ebata, T.; Mikami, N.; Ito, M. *Chem. Phys. Lett.* **1983**, *101*, 578.

(9) Ernstbrunner, E. E.; Girling, R. B.; Grossman, W. E. L.; Hester, R. E. *J. Chem. Soc., Faraday Trans. 2* **1978**, *74*, 501.

(10) Merlin, J. C.; Lorriaux, J. L.; Hester, R. E. *J. Raman Spectrosc.* **1981**, *11*, 384.

(11) Gonohe, N.; Yatsuda, N.; Mikami, N.; Ito, M. *Bull. Chem. Soc. Jpn.* **1982**, *55*, 2796.

(12) Consalvo, D.; Drabbels, M.; Berden, G.; Meerts, W. L.; Parker, D. H.; Reuss, J. *Chem. Phys.* **1993**, *174*, 267.

(13) Parker, D. H.; Avouris, P. *J. Chem. Phys.* **1979**, *71*, 1241.

(14) Galasso, V. *Chem. Phys.* **1997**, *215*, 183.

(15) Avouris, P.; Rossi, A. R. *J. Phys. Chem.* **1981**, *85*, 2340.

(16) Frisch, M. J.; Trucks, G. W.; Schlegel, H. B.; Gill, P. M. W.; Johnson, B. G.; Robb, M. A.; Cheeseman, J. R.; Keith, T.; Petersson, G. A.; Montgomery, J. A.; Raghavachari, K.; Al-Laham, M. A.; Zakrzewski, V. G.; Ortiz, J. V.; Foresman, J. B.; Cioslowski, J.; Stefanov, B. B.; Nanayakkara, A.; Challacombe, M.; Peng, C. Y.; Ayala, P. Y.; Chen, W.; Wong, M. W.; Andres, J. L.; Replogle, E. S.; Gomperts, R.; Martin, R. L.; Fox, D. J.; Binkley, J. S.; Defrees, D. J.; Baker, J.; Stewart, J. J. P.; Head-Gordon, M.; Gonzalez, C.; Pople, J. A. *Gaussian 94*, Gaussian, Inc.: Pittsburgh, PA, 1995.

(17) Becke, A. D. *Phys. Rev. A* **1988**, *38*, 3098.

(18) Becke, A. D. *J. Chem. Phys.* **1993**, *98*, 5648.

(19) Lee, C.; Yang, W.; Parr, R. G. *Phys. Rev. B* **1988**, *37*, 785.

(20) Tannor, D. J.; Heller, E. J. *J. Chem. Phys.* **1982**, *77*, 202.

(21) Halpern, A. M.; Forsyth, D. A.; Nosowitz, M. *J. Phys. Chem.* **1986**, *90*, 2677.

(22) Shida, T.; Nosaka, Y.; Kato, T. *J. Phys. Chem.* **1978**, *82*, 695.

(23) Yokozeki, A.; Kuchitzu, K. *Bull. Chem. Soc. Jpn.* **1971**, *44*, 72.

(24) Hoffmann, R. *Acc. Chem. Res.* **1971**, *4*, 1.

(25) Heilbronner, E.; Muszkat, K. A. *J. Am. Chem. Soc.* **1970**, *92*, 3818.

(26) Nelsen, S. F.; Buschek, J. M. *J. Am. Chem. Soc.* **1974**, *96*, 7930.

(27) Nelsen, S. F.; Hintz, P. J. *J. Am. Chem. Soc.* **1972**, *94*, 7114.

(28) Consalvo, D.; Oomens, J.; Parker, D. H.; Reuss, J. *Chem. Phys.* **1992**, *163*, 223.

(29) Doktorov, E. V.; Malkin, I. A.; Man'ko, V. I. *J. Mol. Spectrosc.* **1977**, *64*, 302.

(30) Vauthey, E.; Henseler, A. *J. Phys. Chem.* **1996**, *100*, 170.

(31) Allonas, X.; Jacques, P. *Chem. Phys.* **1997**, *215*, 371.

(32) Brouwer, A. M. *J. Phys. Chem. A* **1997**, *101*, 3626.

(33) McDivitt, J. R.; Humprey, G. L. *Spectrochim. Acta* **1974**, *30A*, 1021.

(34) Quesada, M. A.; Wang, Z. W.; Parker, D. H. *J. Phys. Chem.* **1986**, *90*, 219.

(35) Marzocchi, M. P.; Sbrana, G.; Zerbi, G. *J. Am. Chem. Soc.* **1965**, *87*, 1429.

(36) Parker, D. H.; Avouris, P. *Chem. Phys. Lett.* **1978**, *53*, 515.